ISSN 1063-7788, Physics of Atomic Nuclei, 2008, Vol. 71, No. 1, pp. 27–35. © Pleiades Publishing, Ltd., 2008.
Original Russian Text © N.A. Demekhina, G.S. Karapetyan, 2008, published in Yadernaya Fizika, 2008, Vol. 71, No. 1, pp. 28–36.

Multimode Approximation for ^{238}U Photofission at Intermediate Energies

N. A. Demekhina* and G. S. Karapetyan[1)]

Yerevan Physics Institute, ul. Brat'ev Alikhanyan 2, Yerevan, 375036 Armenia

Received November 8, 2006; in final form, March 1, 2007

Abstract—The yields of products originating from ^{238}U photofission are measured at the bremsstrahlung endpoint energies of 50 and 3500 MeV. Charge and mass distributions of fission fragments are obtained. Symmetric and asymmetric channels in ^{238}U photofission are singled out on the basis of the model of multimode fission. This decomposition makes it possible to estimate the contributions of various fission components and to calculate the fissilities of ^{238}U in the photon-energy regions under study.

PACS numbers: 25.85.Jg
DOI: 10.1134/S1063778808010031

1. INTRODUCTION

In recent years, much attention has been given in nuclear-fission physics to interpreting mass–energy distributions of fragments within the concept of a multimode character of the decay of nuclei. A piece of evidence that this concept may be realistic comes from the early studies reported in [1–3] and devoted to measuring symmetric and asymmetric components in the mass distribution of fission fragments. Theoretical-model predictions [4, 5] obtained with allowance for the special features of the potential-energy surface and the deformation of a fissile nuclear system, as well as with allowance for the dynamics of the process and the structure of participant nuclei, were confirmed by experimental investigations of charge, mass, and energy distributions of fragments originating from the fission of Po to Fm nuclei that is induced by particles of various type [6–9]. The results of calculations in which one represents fission-product yields as a superposition of symmetric and asymmetric components made it possible to explain basic regularities in the mass and energy distributions of fission fragments. Although the connection between the most probable fission channel and dominant nuclear configurations at the scission point has long since been recognized, deeper insight into the fission process itself could be facilitated only upon developing a general theory for calculating basic properties of deformed nuclear systems. Since the energy and nuclear features of a fissile system determine the relationship between different fission components, it is legitimate to apply model predictions to identical systems whose production was initiated by different projectiles. In the present study, the predictions of the multimode-fission model are first used to analyze mass production in the photofission process. Relations between different fission components make it possible to study the mechanism of the process induced by the interaction with low- and intermediate-energy photons.

The nuclear-fission phenomenon has been studied by various methods (see, for example, [10–12]). The induced-activity method is one the ways to study charge and mass distributions of fission fragments with allowance for their nuclear properties. In the present article, we report on the results of measurements of fission-fragment yields by the induced-activity method that employs the properties of the radioactive decays of reaction products to identity them.

2. EXPERIMENTAL PROCEDURE

The yields of photofission fragments were measured by using a photon beam obtained at the Yerevan synchrophasotron from electrons accelerated to 50 or 3500 MeV. An electron beam was transformed into bremsstrahlung photons by means of a tungsten converter. Irradiated uranium targets of thickness 75 μm had a natural isotopic composition. The photon-beam intensity at the maximum energy of 3500 MeV was determined with a Wilson quantameter. The result was 10^{11} equivalent photons per second. By using monitor reactions, the photon-beam intensity at the maximum energy of 50 MeV was found to be 10^9 equivalent photons per second.

The yields of radioactive fission fragments were measured in the off-line mode by means of a HpGe

[1)]Yerevan State University, ul. Arama Manukyana 1, Yerevan, 375049 Armenia.
*E-mail: demekhina@lnr.jinr.ru

semiconductor detector. The spectrometer resolution and efficiency were determined by using ^{57,60}Co and ^{137}Cs calibration sources and the monitor reactions Al(γ, $2pn$)^{24}Na, ^{12}C$(\gamma,n)^{11}$C, and ^{238}U$(\gamma,n)^{237}$U. The detector resolution was 0.2% at an energy of 1000 keV. The measurements of gamma-ray spectra started after a lapse of ten minutes from the completion of irradiation and continued for a year. The energies of gamma transitions and the relations between their intensities, as well as half-lives, were used to select reaction products and to determine their yields. The reaction-product yield was determined as

$$\sigma = \frac{\Delta N \lambda}{N_\gamma N_n k \epsilon \eta (1 - e^{-\lambda t_1}) e^{-\lambda t_2} (1 - e^{-\lambda t_3})}, \qquad (1)$$

where σ is the yield of the isotope under study per equivalent photon, ΔN is the area under the relevant photopeak, N_γ is the photon-beam intensity (in equivalent photons per second), N_n is the number of target nuclei (in 1/cm^2 units), t_1 is the irradiation time, t_2 is the time interval between the completion of the irradiation and the commencement of the measurements, t_3 is the time of the measurements, λ is the decay constant (in inverse seconds), η is the relative intensity of gamma transitions, k is the total coefficient of gamma-ray absorption in target and detector materials, and ϵ is the gamma-ray-detection efficiency.

Direct isotope production in the reaction being studied is usually considered as an independent yield (I), which is determined by formula (1). If the yield of a given isotope receives a contribution from the β^- or the β^+ decay of neighboring unstable isobars, the respective calculation becomes more complicated [13, 14]. If the formation probability for the parent isotope is known from experimental data or if it can be estimated on the basis of other sources, then the independent yields of daughter nuclei can be calculated by the relation

$$\sigma_B = \frac{\lambda_B}{(1 - e^{-\lambda_B t_1}) e^{-\lambda_B t_2} (1 - e^{-\lambda_B t_3})} \qquad (2)$$
$$\times \left[\frac{\Delta N}{N_\gamma N_n k \epsilon \eta} - \sigma_A f_{AB} \frac{\lambda_A \lambda_B}{\lambda_B - \lambda_A} \right.$$
$$\times \left(\frac{(1 - e^{-\lambda_A t_1}) e^{-\lambda_A t_2} (1 - e^{-\lambda_A t_3})}{\lambda_A^2} \right.$$
$$\left.\left. - \frac{(1 - e^{-\lambda_B t_1}) e^{-\lambda_B t_2} (1 - e^{-\lambda_B t_3})}{\lambda_B^2} \right) \right],$$

where the subscripts A and B label variables referring to, respectively, the parent and the daughter nucleus; the coefficient f_{AB} specifies the fraction of A nuclei decaying to a B nucleus; and ΔN is the total photopeak area associated with the decays of the daughter and parent isotopes. The effect of the precursor can be disregarded in some limiting cases—for example, in the case where the half-life of the parent nucleus is very long or in the case where the fraction of its contribution is very small.

If there are no data on the radioactive-precursor contribution, it is impossible to separate the daughter isotope, in which case the calculated yields are classified as cumulative (C) ones. Experimental data concerning the yields of fragments originating from uranium fission induced by bremsstrahlung photons of endpoint energy of 50 and 3500 MeV are given in Table 1 and in Figs. 1 and 2. The quoted errors in determining yields received contributions from those associated with the statistical significance of experimental results (not greater than 2 to 3%), those in measuring the target thickness (not greater than 3%), and those in determining the detector efficiency (not greater that 10%).

Since the spectrum of bremsstrahlung photons is continuous, the experimentally measured yields receive contributions from the whole photon spectrum, appearing to be an integral effect. Therefore, the results of the measurements at $E_{\gamma\,\max} = 3500$ MeV include the yields associated with the low-energy region. From a comparison of the data in Figs. 1 and 2, one can clearly see the high-energy contribution—in particular, that in the region of yields of symmetric fission-fragment masses. The above dependence leads to the growth of the ratio of the asymmetric- and symmetric-fission yields, which is known in the literature as the peak/plateau ratio [8, 15, 16].

The ratios of the fission-fragment yields at $E_{\gamma\,\max} = 3500$ MeV and 50 MeV are displayed in Fig. 3. From this figure, one can see that, in the mass range 80–100 amu, which corresponds a light asymmetric peak, the yield ratios grow, on average, by a factor of 1.83 ± 0.27; for symmetric fission (100–130 amu), one observes a growth within a factor of 2.42 ± 0.3; the factor of growth in the region of a heavy asymmetric peak (130–150 amu) is 1.51 ± 0.23. Some excess in the growth of yields in the range 80–100 amu may be due to the shift of the light asymmetric and symmetric peaks toward smaller masses with increasing energy; the yields of symmetric fission fragments grow faster. We would like to emphasize that the overlap of mass regions referring to different fission modes may smear the ratios in question.

3. ANALYSIS

Isobar yields not measured by means of the activation procedure in the off-line mode were estimated

Table 1. Yields of fission fragments

Element	Reaction type	σ, mb per equiv. photon		Element	Reaction type	σ, mb per equiv. photon	
		50 MeV	3500 MeV			50 MeV	3500 MeV
$^{77(m+g)}$Ge	C	0.45 ± 0.45	1.481 ± 0.15	^{99g}Rh	C	0.082 ± 0.008	0.13 ± 0.013
^{80}Sr	C	0.08 ± 0.012	0.15 ± 0.015	^{99m}Rh	C	0.23 ± 0.034	0.43 ± 0.043
$^{82(m+g)}$Br	I	0.35 ± 0.049	0.53 ± 0.053	^{101}Tc	C	1.12 ± 0.17	1.73 ± 0.26
$^{82(m+g)}$Sr	C	0.08 ± 0.016	0.014 ± 0.028	^{101m}Rh	I	0.37 ± 0.037	0.69 ± 0.069
^{85m}Kr	C	2.03 ± 0.203	2.25 ± 0.225	^{101}Pd	C	0.72 ± 0.11	1.71 ± 0.25
^{85g}Sr	I	≤ 0.06	0.12 ± 0.0144	^{102m}Rh	I	0.23 ± 0.023	0.5 ± 0.075
^{85m}Sr	I	0.1 ± 0.01	0.19 ± 0.019	^{103}Ru	C	6.73 ± 0.67	11.82 ± 1.18
^{85g}Y	C	≤ 0.009	0.01 ± 0.002	$^{103(m+g)}$Ag	C	0.24 ± 0.024	0.61 ± 0.061
^{85m}Y	C	≤ 0.055	0.08 ± 0.016	^{104g}Ag	I	0.28 ± 0.042	0.31 ± 0.037
^{86}Zr	C	0.067 ± 0.01	0.17 ± 0.017	^{104m}Ag	C	≤ 0.22	0.33 ± 0.049
^{87}Kr	C	1.95 ± 0.195	3.11 ± 0.311	^{104}Cd	C	0.042 ± 0.004	0.15 ± 0.015
^{87m}Sr	I	0.076 ± 0.0076	0.16 ± 0.024	^{105}Ru	C	2.83 ± 0.28	9.63 ± 0.96
^{87g}Y	I	0.02 ± 0.0024	0.052 ± 0.0078	$^{105(m+g)}$Rh	I	0.65 ± 0.065	1.50 ± 0.15
^{87m}Y	C	0.038 ± 0.0057	0.104 ± 0.0156	$^{105(m+g)}$Ag	I	0.24 ± 0.024	0.43 ± 0.043
^{88}Kr	C	1.51 ± 0.151	2.40 ± 0.24	^{106m}Rh	C	0.37 ± 0.037	0.65 ± 0.065
$^{89(m+g)}$Nb	C	0.12 ± 0.018	0.26 ± 0.039	^{106m}Ag	I	0.014 ± 0.002	0.03 ± 0.006
$^{90(m+g)}$Nb	I	≤ 0.02	0.04 ± 0.006	$^{109(m+g)}$In	C	≤ 0.08	0.20 ± 0.03
^{91}Sr	C	5.42 ± 0.542	10.40 ± 1.04	^{109}Sn	C	≤ 0.012	≤ 0.04
^{91g}Y	I	1.29 ± 0.19	2.16 ± 0.22	^{110m}Ag	I	0.29 ± 0.035	0.90 ± 0.09
^{91m}Y	I	0.89 ± 0.13	1.56 ± 0.16	^{110g}In	I	≤ 0.04	≤ 0.07
^{92}Sr	C	5.25 ± 0.53	9.46 ± 0.95	^{111g}Pd	C	1.68 ± 0.17	2.42 ± 0.36
^{92}Y	I	2.12 ± 0.25	2.83 ± 0.34	^{111m}Pd	I	0.91 ± 0.09	1.33 ± 0.13
^{93}Y	C	7.40 ± 0.74	10.54 ± 1.05	$^{111(m+g)}$Ag	C	0.27 ± 0.04	0.63 ± 0.09
^{93m}Mo	C	0.40 ± 0.04	0.45 ± 0.045	^{112}Pd	C	1.79 ± 0.18	6.50 ± 0.65
^{93g}Tc	C	≤ 0.10	0.155 ± 0.019	^{112}Ag	I	0.65 ± 0.13	2.70 ± 0.27
^{93m}Tc	C	≤ 0.23	0.25 ± 0.03	$^{113(m+g)}$Ag	C	2.20 ± 0.33	6.32 ± 0.63
^{95}Zr	C	9.21 ± 0.92	12.50 ± 1.25	^{113m}In	C	0.078 ± 0.01	0.20 ± 0.02
^{95g}Nb	I	0.65 ± 0.065	1.18 ± 0.12	$^{115(m+g)}$Ag	C	1.66 ± 0.33	4.50 ± 0.45
^{95m}Nb	I	1.22 ± 0.18	2.41 ± 0.24	^{115g}Cd	I	0.53 ± 0.11	1.47 ± 0.22
^{95g}Tc	I	≤ 0.14	≤ 0.34	^{115}Sb	C	0.09 ± 0.01	0.17 ± 0.017
^{95m}Tc	I	0.18 ± 0.03	0.42 ± 0.08	^{117g}Cd	C	0.30 ± 0.03	1.12 ± 0.11
^{95}Ru	C	0.04 ± 0.006	0.09 ± 0.009	^{117m}Cd	C	0.52 ± 0.10	2.27 ± 0.23
^{96}Nb	I	0.74 ± 0.07	1.48 ± 0.15	^{117g}In	C	0.40 ± 0.08	1.12 ± 0.08
^{96g}Tc	I	0.04 ± 0.008	0.12 ± 0.02	^{117m}In	I	≤ 0.30	0.55 ± 0.066
^{96m}Tc	I	0.11 ± 0.02	0.29 ± 0.06	^{117m}Sn	C	≤ 0.023	0.054 ± 0.008
^{97}Zr	C	8.20 ± 0.82	10.76 ± 1.10	$^{118(m+g)}$Sb	I	≤ 0.006	≤ 0.019
^{97}Nb	I	0.71 ± 0.14	1.43 ± 0.14	^{119g}Te	C	≤ 0.058	≤ 0.27
^{99}Mo	C	6.50 ± 0.65	8.23 ± 0.82	^{119m}Te	I	≤ 0.053	≤ 0.25
^{99m}Tc	I	1.21 ± 0.12	1.92 ± 0.19	^{120g}I	I	0.046 ± 0.007	0.06 ± 0.006

Table 1. (Contd.)

Element	Reaction type	σ, mb per equiv. photon 50 MeV	3500 MeV	Element	Reaction type	σ, mb per equiv. photon 50 MeV	3500 MeV
^{120m}I	I	0.046 ± 0.007	0.20 ± 0.02	$^{132(m+g)}$La	C	0.13 ± 0.02	0.23 ± 0.023
^{120}Xe	C	0.013 ± 0.003	0.016 ± 0.003	^{132}Ce	C	0.10 ± 0.015	0.16 ± 0.024
^{121g}Te	I	0.14 ± 0.021	0.54 ± 0.081	^{133m}Te	C	2.33 ± 0.23	2.54 ± 0.25
^{121m}Te	I	0.20 ± 0.03	0.64 ± 0.09	$^{133(m+g)}$I	C	8.70 ± 0.87	9.25 ± 0.93
^{121}I	I	0.11 ± 0.017	0.30 ± 0.04	^{133m}Ba	I	0.10 ± 0.01	0.23 ± 0.02
^{121}Xe	C	≤ 0.071	≤ 0.015	^{133}La	I	0.027 ± 0.005	0.064 ± 0.006
$^{122(m+g)}$Sb	C	0.32 ± 0.032	1.39 ± 0.14	^{134}Te	C	2.65 ± 0.27	2.75 ± 0.28
^{123m}Sn	C	1.10 ± 0.11	3.60 ± 0.36	$^{134(m+g)}$I	I	6.42 ± 0.64	6.79 ± 0.68
^{123m}Te	I	0.12 ± 0.018	0.50 ± 0.05	^{134m}Cs	I	≤ 0.05	≤ 0.08
^{123}I	C	0.36 ± 0.054	0.62 ± 0.09	^{135}I	C	6.38 ± 0.64	6.80 ± 0.68
$^{124(m+g)}$Sb	I	1.36 ± 0.136	2.33 ± 0.233	$^{135(m+g)}$Xe	I	2.16 ± 0.22	2.82 ± 0.28
$^{124(m+g)}$I	I	0.60 ± 0.06	0.90 ± 0.09	^{135m}Cs	I	≤ 0.63	≤ 0.75
^{125g}Sn	C	0.80 ± 0.08	3.56 ± 0.36	^{135m}Ba	I	≤ 0.06	≤ 0.07
$^{125(m+g)}$Xe	C	0.15 ± 0.02	0.54 ± 0.06	^{137g}Ce	C	5.48 ± 0.54	8.31 ± 0.83
$^{126(m+g)}$Sb	I	1.60 ± 0.16	2.48 ± 0.25	^{137m}Ce	C	1.02 ± 0.10	1.33 ± 0.13
$^{126(m+g)}$I	I	0.70 ± 0.07	1.91 ± 0.19	$^{137(m+g)}$Nd	C	0.31 ± 0.06	0.55 ± 0.07
^{126}Ba	C	0.049 ± 0.005	0.09 ± 0.009	^{139}Ba	C	1.08 ± 0.11	2.66 ± 0.27
$^{127(m+g)}$Sn	C	1.35 ± 0.14	2.52 ± 0.25	^{140}Ba	C	6.26 ± 0.63	7.04 ± 0.84
^{127}Sb	C	1.24 ± 0.12	4.14 ± 0.41	^{140}La	I	2.18 ± 0.22	2.45 ± 0.25
$^{127(m+g)}$Xe	I	0.048 ± 0.005	0.11 ± 0.011	^{141}La	I	3.77 ± 0.38	5.09 ± 0.51
^{127}Cs	C	≤ 0.19	≤ 0.40	^{141}Ce	C	1.91 ± 0.32	3.91 ± 0.32
$^{128(m+g)}$Sn	C	1.30 ± 0.13	3.20 ± 0.32	^{142}La	C	1.48 ± 0.22	2.40 ± 0.24
$^{128(m+g)}$Sb	I	1.35 ± 0.14	3.90 ± 0.39	^{143}Ce	C	4.30 ± 0.43	5.12 ± 0.52
$^{128(m+g)}$I	I	≤ 0.35	≤ 0.82	^{146}Gd	C	0.07 ± 0.014	0.10 ± 0.02
^{128}Ba	C	≤ 0.024	0.067 ± 0.007	^{147}Nd	C	0.60 ± 0.09	1.50 ± 0.15
^{129}Sb	C	3.11 ± 0.31	3.93 ± 0.39	$^{147(m+g)}$Tb	C	≤ 0.09	≤ 0.186
$^{129(m+g)}$Te	I	0.91 ± 0.09	1.45 ± 0.15	^{148g}Pm	I	≤ 0.128	≤ 0.20
^{129m}Xe	I	0.076 ± 0.008	0.12 ± 0.018	^{148m}Pm	I	≤ 0.19	≤ 0.32
^{129}Cs	I	≤ 0.009	≤ 0.016	^{148}Eu	I	0.08 ± 0.012	0.15 ± 0.015
^{130g}Sb	C	1.43 ± 0.14	1.58 ± 0.16	$^{148(m+g)}$Tb	C	≤ 0.06	≤ 0.08
$^{130(m+g)}$I	I	0.47 ± 0.05	1.18 ± 0.12	^{149}Nd	C	0.56 ± 0.067	1.12 ± 0.12
^{131}Sb	C	1.47 ± 0.15	2.14 ± 0.25	^{149}Gd	C	0.26 ± 0.039	0.51 ± 0.051
^{131g}Te	C	2.32 ± 0.23	2.82 ± 0.42	$^{149(m+g)}$Tb	C	0.03 ± 0.006	0.06 ± 0.012
^{131m}Te	I	3.16 ± 0.32	3.80 ± 0.38	^{150}Pm	I	0.44 ± 0.088	0.54 ± 0.081
^{131}I	I	2.70 ± 0.27	3.47 ± 0.35	^{150m}Eu	I	≤ 0.23	≤ 0.25
$^{131(m+g)}$Ba	C	0.029 ± 0.004	0.043 ± 0.006	$^{150(m+g)}$Tb	C	≤ 0.08	≤ 0.11
^{132}Te	C	5.71 ± 0.57	6.23 ± 0.62	^{151}Nd	C	0.34 ± 0.051	0.44 ± 0.066
^{132g}I	I	0.95 ± 0.10	0.98 ± 0.10	^{151}Pm	I	≤ 0.21	≤ 0.29
^{132m}I	I	2.94 ± 0.29	3.35 ± 0.34	$^{151(m+g)}$Tb	C	≤ 0.05	≤ 0.07
^{132}Cs	I	≤ 0.39	≤ 0.78				

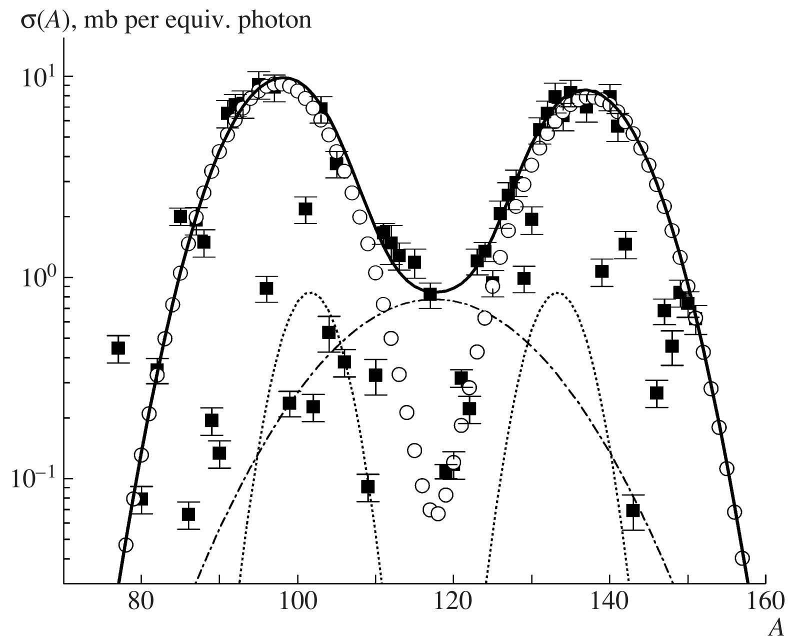

Fig. 1. Component of the mass yield at $E_{\gamma_{\max}} = 50$ MeV: (dash-dotted curve) "Superlong," (dotted curve) "Standard I," and (open circles) "Standard II." The total yield $Y_{\rm tot}$ and experimental data are represented by the solid curve and closed boxes, respectively.

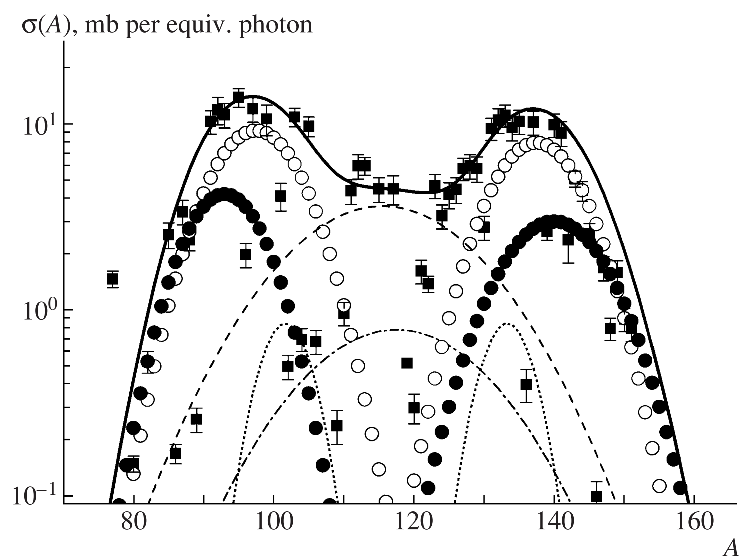

Fig. 2. Mass yield at $E_{\gamma_{\max}} = 3500$ MeV. The notation for the yields from low-energy fission is identical to that in Fig. 1. For high-energy fission, the closed circles, dashed curve, and solid curve represent, respectively, the asymmetric mode, symmetric mode, and total yield. The closed boxes stand for experimental data.

with the aid of a Gaussian function, which is usually used to approximate charge distributions [17]; that is,

$$\sigma(A,Z) = \frac{\sigma(A)}{(C\pi)^{1/2}} \exp\left[-\frac{(Z-Z_p)^2}{C}\right], \quad (3)$$

where $\sigma(A,Z)$ is the measured independent yield of a fragment whose charge and mass numbers are Z and A, respectively. In the fitting procedure, $\sigma(A)$ (total yield at a given mass number A), Z_p (most probable charge in the distribution in question), and C (width parameter of the charge distribution) were treated as adjustable parameters.[2)]

The values calculated for $\sigma(A)$, which correspond

[2)]The behavior of these parameters is not discussed in the present article.

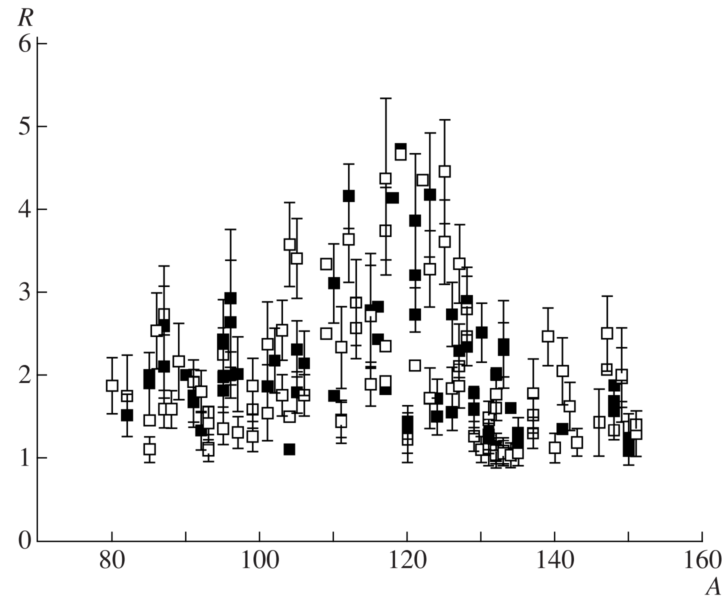

Fig. 3. Ratio R of the yields of fission fragments: (closed boxes) independent yields and (open boxes) cumulative yields.

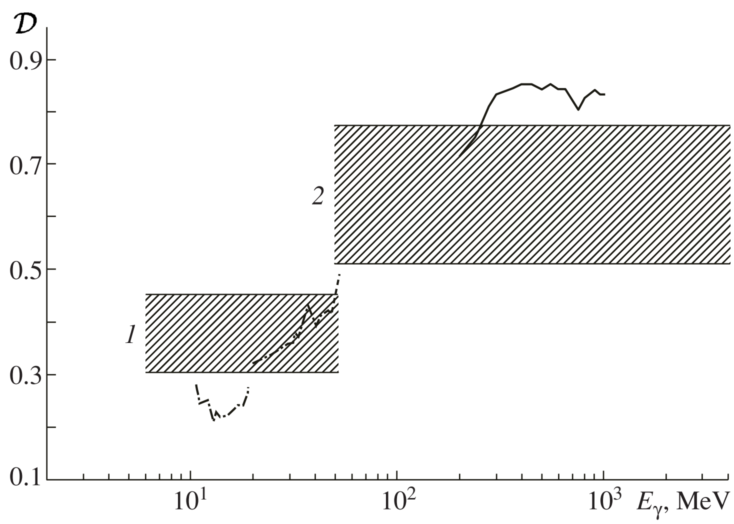

Fig. 4. Fissility $\mathcal{D}$: (shaded regions) our present data [(*1*) $6 \leq E_\gamma \leq 50$ MeV and (*2*) $50 \leq E_\gamma \leq 3500$ MeV], (dash-dotted curve) data from [18], and (solid curve) data from [24].

to the total yield of fission fragments characterized by a given mass number, made it possible to construct the mass distribution of fission fragments at two endpoint energies of the bremsstrahlung spectra. These results are represented by the solid curves in Figs. 1 and 2. We calculated the total yield from uranium photofission as the sum of the yields of all specific fission products, considering that two fragments are formed in one event: $Y_{\text{tot}} = \sum_A \sigma(A)$ (Table 2). For the sake of comparison, data from the literature [18–21] are also quoted in Table 2. Because of the interaction with bremsstrahlung photons, the total photofission yield is determined by the endpoint energy of the spectrum, and the energy dependence of the photofission cross section is in fact reflected in the pattern of the mass distribution of fission fragments. In the case being considered, one can therefore trace changes in the photofission mechanism with increasing energy by representing total yields as the sum of different mass components.

We will discuss the mass yield of fission fragments on the basis of the multimode-fission concept [4, 5]. According to this hypothesis, the mass-yield curve can be described as a superposition of several components that take into account symmetric and asymmetric channels of the decay of a nucleus

Table 2. Yields from symmetric, asymmetric, and total fission (in millibarns per equivalent photon)

Yield	50 MeV	3500 MeV
Y_{tot}	131.6 ± 19.5	250.1 ± 37.5
	$\sim$120 [18, 19]	251 ± 25 [20]
Y_{s}	10.6 ± 1.5	79.3 ± 11.9
Y_{as}	121.0 ± 18.0	170.8 ± 25.6
$Y_{\text{as/s}}$	11.41 ± 1.71	2.16 ± 0.40
peak/plateau	11.36 ± 1.70	2.40 ± 0.36
ratio	11 [21]	1.8 [21]

undergoing fission as it traverses the scission point. In implementing this approach, yields associated with different fission modes are represented in the form of Gaussian functions whose parameters determine basic nuclear properties of mass distributions of fission fragments [6].

Using data associated with low-energy fission [6, 8, 11], we decomposed the total photofission yield at the energy of 50 MeV, $Y_{\text{tot}} = Y_1$, into individual terms representing one symmetric (Superlong) and two asymmetric (Standard I and Standard II) fission modes.

The above decomposition was performed by approximating the mass-yield curve in the form of a superposition of the aforementioned components; that is,

$$\begin{aligned} Y_1 = {} & \frac{K_{1\text{as}}}{\sigma_{1\text{as}}\sqrt{2\pi}} \exp\left[-\frac{(A - \bar{A}_{1\text{s}} - D_{1\text{as}})^2}{2\sigma_{1\text{as}}^2}\right] \\ & + \frac{K'_{1\text{as}}}{\sigma'_{1\text{as}}\sqrt{2\pi}} \exp\left[-\frac{(A - \bar{A}_{1\text{s}} + D_{1\text{as}})^2}{2\sigma'^2_{1\text{as}}}\right] \\ & + \frac{K_{2\text{as}}}{\sigma_{2\text{as}}\sqrt{2\pi}} \exp\left[-\frac{(A - \bar{A}_{1\text{s}} - D_{2\text{as}})^2}{2\sigma_{2\text{as}}^2}\right] \\ & + \frac{K'_{2\text{as}}}{\sigma'_{2\text{as}}\sqrt{2\pi}} \exp\left[-\frac{(A - \bar{A}_{1\text{s}} + D_{2\text{as}})^2}{2\sigma'^2_{2\text{as}}}\right] \\ & + \frac{K_{1\text{s}}}{\sigma_{1\text{s}}\sqrt{2\pi}} \exp\left[-\frac{(A - \bar{A}_{1\text{s}})^2}{2\sigma_{1\text{s}}^2}\right], \end{aligned} \tag{4}$$

where each component is characterized by the mean mass number $\bar{A}$, the variance σ, the Gaussian-function parameter D, and the normalization factor K [6].

In order to attain a higher physical reliability of computed data, we employed, in addition to the standard criterion specified by the χ^2 value (which is equal to 1.12), some additional conditions confirming agreement with experimental data. These require (i) that, within the measurement errors, the total yield Y_1 determined by summing all components agree with experimental data at the photon endpoint energy of $E_{\gamma\,\max} = 50$ MeV and (ii) that the channel ratio for symmetric and asymmetric fission modes agree with the peak/plateau ratio measured experimentally.

Table 3. Fitted values of the parameters in Eqs. (5) and (6)

Parameter	50 MeV	3500 MeV
$K_{1\text{as}}$	7.5 ± 0.04	7.5 ± 0.04
$K'_{1\text{as}}$	7.5 ± 0.04	7.5 ± 0.04
$K_{2\text{as}}$	120.0 ± 6.0	120.0 ± 6.0
$K'_{2\text{as}}$	140.0 ± 7.2	140.0 ± 7.2
$K_{1\text{s}}$	23.75 ± 0.7	23.75 ± 0.7
$K_{2\text{s}}$	–	112.0 ± 4.5
$K_{3\text{as}}$	–	52.75 ± 2.11
$K'_{3\text{as}}$	–	74.0 ± 3.0
$\sigma_{1\text{as}}$	3.54 ± 0.4	3.54 ± 0.4
$\sigma'_{1\text{as}}$	3.54 ± 0.4	3.54 ± 0.4
$\sigma_{2\text{as}}$	6.0 ± 0.21	6.0 ± 0.21
$\sigma'_{2\text{as}}$	6.0 ± 0.21	6.0 ± 0.21
$\sigma_{1\text{s}}$	12.0 ± 0.48	12.0 ± 0.48
$\sigma_{2\text{s}}$	–	12.35 ± 0.5
$\sigma_{3\text{as}}$	–	7.0 ± 0.111
$\sigma'_{3\text{as}}$	–	5.4 ± 0.08
$\bar{A}_{1\text{s}}$	117.5 ± 0.2	117.5 ± 0.2
$\bar{A}_{2\text{s}}$	–	116.5 ± 0.24
$D_{1\text{as}}$	15.82 ± 1.01	15.82 ± 1.01
$D_{2\text{as}}$	20.0 ± 1.4	20.0 ± 1.4
$D_{3\text{as}}$	–	23.5 ± 0.99

The results of the calculations made it possible to determine the positions of the peaks, the variances, and the contribution of each fission mode to the total mass yield.

Considering that, with increasing energy, the yields of fission fragments grow both in the region of symmetric and in the region of asymmetric masses (Fig. 2), we supplemented the decomposition of the mass yield at the energy of 3500 MeV with a symmetric and an asymmetric component; that is,

$$Y_2 = Y_1 + Y', \tag{5}$$

$$Y' = \frac{K_{2\text{s}}}{\sigma_{2\text{s}}\sqrt{2\pi}} \exp\left[-\frac{(A - \bar{A}_{2\text{s}})^2}{2\sigma_{2\text{s}}^2}\right] \tag{6}$$

$$+ \frac{K_{3\mathrm{as}}}{\sigma_{3\mathrm{as}}\sqrt{2\pi}} \exp\left[-\frac{(A - \bar{A}_{2\mathrm{s}} - D_{3\mathrm{as}})^2}{2\sigma_{3\mathrm{as}}^2}\right]$$
$$+ \frac{K'_{3\mathrm{as}}}{\sigma'_{3\mathrm{as}}\sqrt{2\pi}} \exp\left[-\frac{(A - \bar{A}_{2\mathrm{s}} + D_{3\mathrm{as}})^2}{2\sigma'^2_{3\mathrm{as}}}\right],$$

where Y_1 is calculated by formula (4). In the case being considered, the above additional criterion for testing the reliability of the fitting procedure was applied in comparing $Y_2 = Y_1 + Y'$ with experimental data for the photon endpoint energy of 3500 MeV. Accordingly, the peak/plateau ratio was also used in that energy region. The fitted values of the parameters that determine the components of the mass-yield curves (at $\chi^2 = 1.2$) are given in Table 3.

4. RESULTS AND DISCUSSION

Our investigation made it possible to determine the photofission yield in the region of intermediate energies (above the giant resonance) and to estimate the fissility parameter. According to the well-known concept, the fissility parameter is determined as the ratio of the fission yield and the yield of total photon absorption in a nucleus ($D = Y_{\mathrm{tot}}/Y_{\mathrm{abs}}$). In determining Y_{abs}, it is necessary to take into account all possible channels of decay of the excited nucleus being considered.

In the giant-resonance region, photon interaction with uranium nuclei is accompanied predominantly by the emission of one or two neutrons or by fission. We calculated Y_{abs} using the results of our measurements of the yield from the relevant (γ, n) reaction and data from the literature on the respective $(\gamma, 2n)$ reaction [18].

In the region of intermediate energies (50–3500 MeV), new channels of decay of an excited nucleus come into play. Experimental data and model calculations from [22, 23] were used to calculate the total-photoabsorption yield in this energy region. The resulting estimates are given in Fig. 4.

From Fig. 4, one can see that the data in question are compatible with the latest results of measurements that were performed in this energy region with monoenergetic photons [24]. The fissility of uranium proved to be less than unity and increased up to a value of 0.64 ± 0.13 upon going over from low to intermediate energies.

As is well known, the excitation energy of nuclei undergoing fission plays an important role in fission dynamics. Asymmetric fission, which is due largely to the effect of nuclear shells [4], is dominant at low excitation energies of fissile nuclei. With increasing energy, the impact of shell effects becomes less pronounced, while the contribution of symmetric binary nuclear decay increases. At these energies, the fission process is described on the basis of the liquid-drop model.

Chung and Hogan [25, 26], who studied the fission of actinide nuclei that is induced by protons of energy in the range extending up to 100 MeV, introduced an empirical expression for the relationship between different fission channels versus the nucleonic composition of a fissile nucleus. In order to characterize this factor quantitatively, they introduced a critical value of the fissility parameter,

$$(Z^2/A)_{\mathrm{as/s}} = 35.5 + 0.4(Z_f - 90), \tag{7}$$

where Z_f is the charge number of the nucleus undergoing fission.

For the ^{238}U nucleus, this parameter is 36.3. For Z^2/A values greater than the critical value, Chung and Hogan [25, 26] assumed that the symmetric fission mode was dominant, but, at smaller values of the fissility parameter, the main fission channel led to asymmetric fragments. At average excitation energies of about 17 to 18 MeV [27], which lie in the giant-resonance region and which lead to the evaporation of not more than two neutrons, it is natural to expect predominantly asymmetric fission.

A significant growth of the symmetric-fission-mode contribution with increasing energy of incident photons is worthy of special note. On average, the yields of the different fission modes in the energy range 50–3500 MeV were $Y_{\mathrm{s}} = 68.7 \pm 10.3$ mb per equivalent photon and $Y_{\mathrm{as}} = 49.8 \pm 7.47$ mb per equivalent photon. In the case of neutron interaction with ^{238}U nuclei at energies in the range extending up to 500 MeV, Zoller et al. [28] also indicated the growth of the symmetric-fission fraction with increasing energy. Calculations on the basis of the statistical model [29] made it possible to estimate the growth of the symmetric-fission contribution with allowance for additional channels of decay of intermediate nuclei formed upon the emission of prefission neutrons.

Within the cascade–evaporation model, an increase in the projectile energy leads to an increase in the excitation energy [30] and, accordingly, to an increase in the number of emitted nucleons. For heavy target nuclei, prefission neutrons constitute the bulk of emitted nucleons (the emission of protons is strongly suppressed), this leading to the formation of a set of neutron-deficient fissile systems.

From our experimental data, it follows that the mass distribution of the symmetric-fission peak at the energy of 3500 MeV has a maximum at $\bar{A}_{2\mathrm{s}} = 116.5$ amu and $Z_p = 46$. Thus, one can see that, presumably, a nucleus undergoes symmetric fission at an average mass-number value of $A_f \approx 233$ amu and a charge number of $Z_f \approx 92$, this corresponding to neutron-deficient uranium isotopes. According to data reported in [15], the probability of fission in the region of intermediate energies has a broad distribution versus the number of emitted neutrons. Therefore, the increase in the symmetric-fission component may be due to the contribution of neutron-deficient fissile nuclear systems.

5. CONCLUSIONS

On the basis of an investigation of the fragment mass yield, the decomposition of the total photofission yield into symmetric and asymmetric components has been constructed for the first time within the multimode pattern of the decay of an excited nucleus. Owing to separating the high-energy component of the yield, we have been able to analyze the character of the dependence of the yield of various fission modes on the excitation energy of the nucleus formed after the completion of the intranuclear cascade. A sharp growth of the symmetric-fission component with increasing photon energy has been found.

ACKNOWLEDGMENTS

We are grateful to the staff of the Yerevan Electron Synchrotron for ensuring the required beam parameters and to V.I. Chepygin from the Laboratory of Nuclear Reactions at the Joint Institute for Nuclear Research (JINR, Dubna) for placing the needed targets at our disposal.

REFERENCES

1. J. P. Unik, J. E. Gindler, L. E. Glendenin, et al., in *Proceedings of the Third International Atomic Energy Agency Symposium on the Physics and Chemistry of Fission, Rochester, 1973*, Vol. 2, p. 191.
2. W. John, E. K. Hulet, R. W. Lougheed, and J. J. Wesolowski, Phys. Rev. Lett. **27**, 45 (1971).
3. E. Konecny and H. W. Schmitt, Phys. Rev. **172**, 1213 (1968).
4. B. D. Wilkins, E. P. Steinberg, and R. R. Chasman, Phys. Rev. C **14**, 1832 (1976).
5. U. Brosa, S. Grossman, and A. Muller, Z. Naturforsch. Teil A **41**, 1341 (1986).
6. W. Younes, J. A. Becker, L. A. Bernstein, et al., in *Proceedings of the International Nuclear Physics Conference (INPC 2001)*, AIP Conf. Proc. **610**, 673 (2002).
7. K.-H. Schmidt et al., Nucl. Phys. A **665**, 221 (2000).
8. T. Ohtsuki, Y. Hamajima, K. Sueki, et al., Phys. Rev. C **40**, 2144 (1989).
9. V. C. Duijvestijn, A. J. Koning, J. P. M. Beijers, et al., Phys. Rev. C **59**, 776 (1999).
10. K. Persyn, S. Pomme, E. Jacobs, et al., in *Proceedings of the Second International Conference on Dynamical Aspects of Nuclear Fission, Smolenice, Slovakia, 1993*; JINR Report No. E7-94-19 (Dubna, 1994), p. 59.
11. R. Kotte et al., Z. Phys. A **330**, 189 (1988).
12. S. D. Beĭzin, S. V. Zhdanov, M. G. Itkins, et al., *Proceedings of the International Conference "Nuclear Fission—50 years", Leningrad, 1989*.
13. H. Baba, J. Sanada, H. Araki, and A. Yokoyama, Nucl. Instrum. Methods Phys. Res. A **416**, 301 (1998).
14. I. Adam, V. S. Pronskikh, A. R. Balabekyan, et al., Preprint No. 10-2000-28, OIYaI (Joint Institute for Nuclear Research, Dubna, 2000).
15. P. David, J. Debrus, U. Kim, et al., Nucl. Phys. A **197**, 163 (1972).
16. D. R. Nethaway and B. Mendoza, Phys. Rev. C **6**, 1827 (1972).
17. H. Kudo, M. Maruyama, M. Tanikawa, et al., Phys. Rev. C **57**, 178 (1998).
18. A. Veyssiere, H. Beil, R. Bergere, et al., Nucl. Phys. A **199**, 45 (1973).
19. H. Ries, U. Kneissl, G. Mank, et al., Phys. Lett. B **139**, 254 (1984).
20. G. A. Vartapetyan, N. A. Demekhina, V. I. Kasilov, et al., Yad. Fiz. **14**, 65 (1971) [Sov. J. Nucl. Phys. **14**, 37 (1971)].
21. B. Schröder, G. Nydahl, and B. Forkman, Nucl. Phys. A **143**, 449 (1970).
22. A. Deppman et al., Phys. G **30**, 1991 (2004).
23. C. Cetina et al., Phys. Rev. C **65**, 044622 (2002).
24. A. Deppman, O. A. P. Tavares, S. B. Duarte, et al., Phys. Rev. C **66**, 067601 (2002).
25. Chien Chung and James J. Hogan, Phys. Rev. C **25**, 899 (1982).
26. Chien Chung and James J. Hogan, Phys. Rev. C **24**, 180 (1981).
27. E. Jacobs, H. Thierens, D. De Frenne, et al., Phys. Rev. C **19**, 422 (1979).
28. C. M. Zoller, A. Gavron, J. P. Lestone, et al., IKDA 95/25 (Darmstadt, 1995).
29. V. M. Maslov, Nucl. Phys. A **717**, 3 (2003).
30. V. S. Barashenkov, F. G. Gereghi, A. S. Iljinov, et al., Nucl. Phys. A **231**, 462 (1974).

Translated by A. Isaakyan